Colorimetric and Resistive Polymer Electrolyte Thin Films for Real-time Humidity Sensors

Eunyeong Kim,[†] Sung Yeon Kim,[‡] Gyuha Jo,[†] Suhan Kim,[§] and Moon Jeong Park*,[†,‡]

[†]Department of Chemistry, [‡]Division of Advanced Materials Science, Pohang University of Science and Technology (POSTECH), Pohang, Korea 790-784

[§]Energy and Environmental Research Division, Research Institute of Industrial Science and Technology (RIST), Pohang, Korea 790-330

S *Supporting Information*

ABSTRACT: We have developed fast responsive, colorimetric and resistive-type polymeric humidity sensors from a series of self-assembled poly(styrenesulfonate-methylbutylene) (PSS-b-PMB) block copolymers with tailored hygroscopic properties. In dry state, the PSS-b-PMB films exhibit hexagonal cylindrical morphology where hydrophobic PMB cylinders are dispersed within a PSS matrix. Under levels of humidity, the PSS-b-PMB thin films self-displayed discernible reflective color changes, covering almost entire visible light regions from violet (RH = 20%) to red (RH = 95%). The sensors also revealed a few orders of magnitude changes in impedance with exposure to humid air by taking advantages of strong polymer electrolytes characteristics. Remarkably, the time to complete the changes in the signals was only a few seconds, as rationalized by good connectivity of the PSS domains and short water diffusion pathways in nanometer scales. Repeated hydration/dehydration tests demonstrated reliable sensor properties, which is in sharp contrast to the poor stability of PSS homopolymer sensors lacking organization.

KEYWORDS: sensors, humidity, stimuli-responsive materials, color, impedance, block copolymer electrolytes
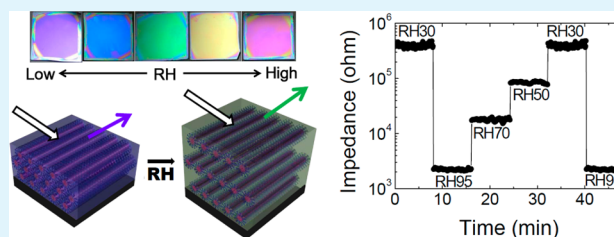
INTRODUCTION

Chemical sensors based on stimuli-responsive materials have been extensively investigated in past decades.[1−3] Among a wide variety of target molecules, accurate and reliable measurements of humidity have attracted great attention in diverse fields of medical science,[4] food industry,[5] and electronic applications.[6] Different types of humidity sensors have been developed from porous ceramics,[7,8] metals,[9,10] and polymeric materials,[11] where the materials exhibit changes in physical properties such as capacity,[12] resistance,[13−15] surface acoustic wave,[16,17] reflection,[18,19] and fluorescent emission,[20,21] upon exposure to moisture.

In the class of humidity-sensitive materials, polymeric materials have particular advantages of flexibility, easy fabrication, and low cost. Especially, polymer electrolytes have been the most widely exploited polymeric materials as resistive-type humidity sensors owing to their ion-conducting characteristics.[22−24] For the polymer electrolytes, polymer-salt complexes,[25,26] and hydrophilic vinyl polymers bearing acid groups[27] or quaternary salts[21,24,28,29] have been commonly used. Several approaches are in progress to tailor the physicochemical properties of polymer electrolytes toward high performance humidity sensors. For example, in an effort to achieve high sensitivity and fast response, the incorporation of hygroscopic ingredients, that is, acid and nanoparticles, into the polymer electrolytes were carried out.[22−24,30,31] However, the

blending often results in sensor drift and poor durability under repeated hydration/dehydration cycles.[22]

Along with the chemical constituents, interestingly, it has been revealed that structural aspects are also important parameters in attaining improved sensor performance under the levels of humidity.[28,29,32,33] The widespread use of photonic crystals in humidity sensors would be a good example of the structural design of polymer electrolytes.[34−40] The photonic crystals exhibit unique structural colors, which can be altered by water sorption, if accompanied by significant changes in lattice spacing. This leads to a visually readable response under indoor illumination, which can make the sensor devices simple by eliminating analytical instruments to measure the signals. Although the photonic crystals have shown promise, large volume changes over a several-fold are essentially required for the recognition of color changes with naked eyes,[41,42] impeding fast response time and good reversibility of the sensors.

Herein, we are motivated to develop fast responsive and highly sensitive polymeric humidity sensors based on rational molecular designs. A set of partially sulfonated poly(styrene-*block*-methylbutylene) block copolymers (hereafter PSS-b-PMB copolymers) have been synthesized where the PSS chains provide hygroscopic nature. The degree of water sorption was

easily tuned by adjusting sulfonation levels of the PSS chains, offering the ability to control sensor performance. The introduction of covalently bonded hydrophobic PMB blocks leads to exclusive self-assembled nanoscale morphologies.[43,44]

Unlike other polymeric humidity sensors reported to date, in present study, we have demonstrated a facile route toward dual-mode humidity sensors with extremely fast response time of a few seconds. The sensors from PSS-b-PMB films displayed discernible reflective colors of violet, blue, green, yellow, orange, and red under levels of humidity with remarkably fast response time of a few seconds. The sensors also confirmed fast substantial impedance changes with the change in humidity by taking advantage of strong polyelectrolyte characteristics. The development of opto-electrochemically responsive humidity sensors in thin film configuration would open promising avenues toward microsensor applications.

■ EXPERIMENTAL SECTION

Synthesis of PSS-b-PMB Copolymers. A set of PSS-b-PMB copolymers with different sulfonation levels (SLs) was prepared according to the procedures in ref 45. A poly(styrene-*b*-isoprene) (PS-b-PI, 9.5−9.1 kg/mol, polydispersity index of 1.02) precursor block copolymer was synthesized by sequential anionic polymerization of styrene and isoprene. The molecular weight and molecular weight distribution of PS-b-PI were characterized by combining [1]H Nuclear Magnetic Resonance (^{1}H NMR, Bruker AVB-300) spectroscopy and gel permeation chromatography (GPC, Waters Breeze 2 HPLC). The saturation of PI chains was performed in the presence of a homogeneous Ni−Al catalyst at 80 °C and 420 psi, followed by the sulfonation reaction of PS blocks. Six different SL values of 29, 35, 42, 49, 60, and 76 mol. % were obtained by controlling sulfonation reaction times where the SL values were calculated by the ratio of moles of sulfonated styrene (after the reaction) to total moles of styrene (before the reaction), determined by ^{1}H NMR spectra with acetone-d_6. The molecular structure of resulting materials is shown in Figure 1a.

Morphology Characterizations. The morphology of the films beneath the surface in position space was investigated by cross-sectional transmission electron microscope (TEM) experiments. The

Figure 1. Molecular structure of (a) poly(styrenesulfonate-b-methylbutylene) (PSS-b-PMB) copolymers and (b) cross-sectional TEM images of P(60) sample representing hexagonally packed hydrophobic PMB cylinders, dispersed in a hydrophilic PSS matrix. The PSS domain was darkened by RuO_4 staining and the scale bars represent 100 nm.

standard technique of delaminating polymer films using an epoxy matrix was employed, followed by cryo-microtoming at −120 °C to obtain sections with thicknesses in the 80−120 nm range using a RMC Boeckeler PT XL Ultramicrotome. The selective staining of PSS phases was accomplished by exposure to ruthenium tetroxide (RuO_4) vapor for 50 min. Imaging of stained samples was performed with a JEOL-2100F microscope operating at 200 kV. Grazing incident small-angle X-ray scattering (GISAXS) experiments were carried out at the beamline 3C, equipped with a charge-coupled device detector (2048 × 2048 pixels) at the Pohang Light Source (PLS). The sample-to-detector distance was 2.76 m and the incident angle was varied from 0.10° to 0.24° in 0.01° increments.

Water Uptake Measurements. Polymer films with thicknesses ca. 5 μm were prepared by solvent casting from 1 wt % THF solutions. The films were dried at room temperature for 3 days under a N_2 blanket and under vacuum at 50 °C for 5 days. The films were located in a benchtop humidity/temperature environmental chamber (JEIO Tech, TH-PE-025). The amounts of water sorption at given relative humidities (RHs) at a fixed temperature of 25 °C were measured using a Mettler balance with 0.01 mg accuracy. The water uptake is calculated using the dry film as the basis

$$\text{water uptake (\%)} = \frac{\text{weight of wet film} - \text{weight of dry film}}{\text{weight of dry film}} \times 100 \qquad (1)$$

The reported water uptake values are based on measurements from 5 independent samples.

Color Observation and Impedance Measurements. Solutions (4 wt %) of PSS-b-PMB copolymers in THF were spin-coated on a Si wafer with a native oxide layer. A variable-angle multiwavelength ellipsometer (Gaertner, L2W16C830) was used to measure the thicknesses and refractive indices of the dried films. The PSS-b-PMB films with thickness of ca. 240 nm were placed in benchtop humidity/temperature environmental chamber (JEIO Tech, TH-PE-025). The changes in reflective color under levels of humidity were monitored in real-time via specially designed transparent window. The impedance of PSS-b-PMB films at each humidity condition was simultaneously measured using a 1260 Solatron impedance analyzer. An ac voltage of 20 mV at a single frequency of 1 kHz was applied to our sensors and the impedance was measured with time. The change in ac voltage in the range of 5−30 mV does not make considerable effects on the impedance results. The frequency of 1 kHz was located in impedance plateau region. For the impedance measurements, interdigitated gold stripes were employed as working and counter electrodes to apply a current to the films where the gold stripes were 300 μm wide and 300 μm apart. A schematic diagram illustrating the interdigitated gold electrode is given in Figure S1 of Supporting Information.

Optical Analysis. Reflectance of PSS-b-PMB films coated on Si-wafers was recorded at 25 °C using a Cary 5000 UV/vis/NIR spectrophotometer (Varian Inc.). The cuvette cell was modified for the humidity experiments. The cell contains salty water in its bottom and PSS-b-PMB films were located inside the cuvette using specially designed supporting mounts. UV Reflectance profiles of PSS-b-PMB films were then analyzed using Essential Macleod software. Because of the scale difference, the intensity spectrum obtained from the simulation was normalized by matching the maximum peak intensity to that obtained experimentally.

■ RESULTS AND DISCUSSION

Morphology of PSS-b-PMB Sensors. Figure 1a shows the chemical structure of PSS-b-PMB copolymers where the subscripts indicate the degree of polymerization of each block. The SL values of PSS-b-PMB copolymers are calculated from the ratio of x to 95, as determined by ^{1}H NMR experiments. For brevity, the samples are labeled only with the SL values. For example, P(35) indicates the PSS-b-PMB copolymer with 95 PS chains and 134 PMB units where 35 mol.% of PS chains (ca. 33 units) is sulfonated. The SL values
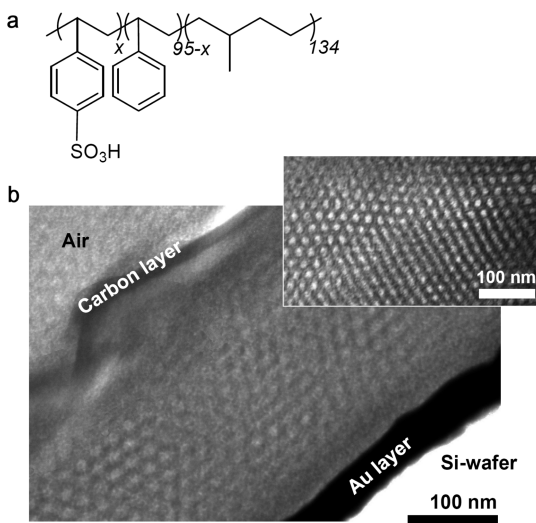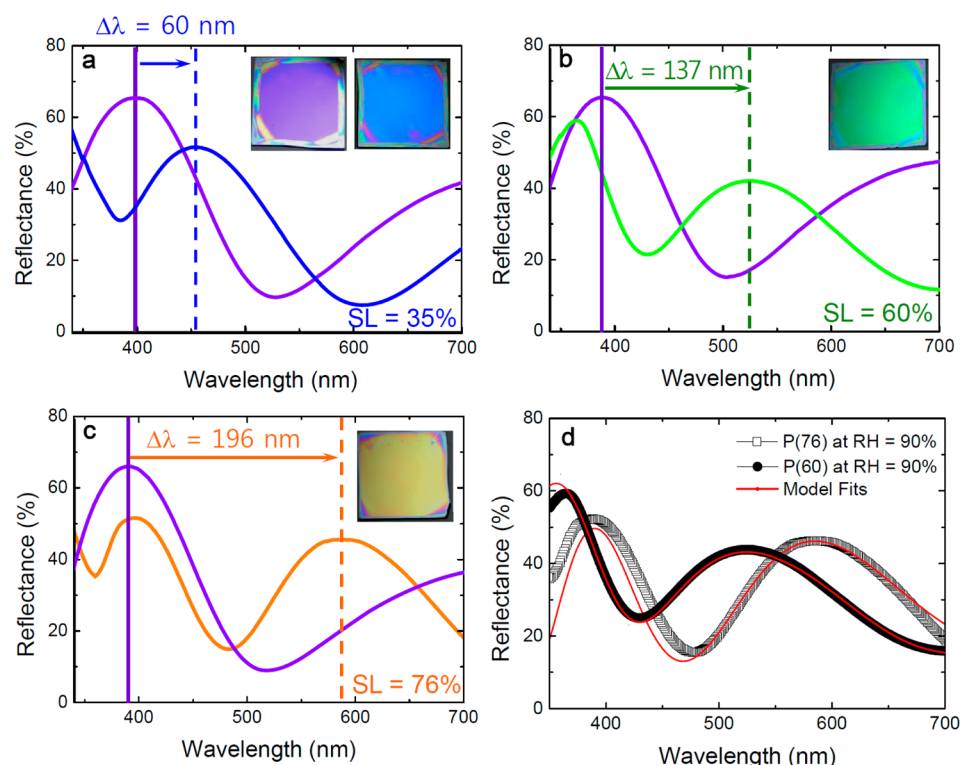
Figure 2. UV−visible reflectance spectra of (a) P(35), (b) P(60), and (c) P(76) thin films with qualitative the same thickness of ∼240 nm under RH = 20% and RH = 90% conditions (T = 25 °C). At RH = 90%, the P(35), P(60), and P(76) films swell to reflect peak wavelength of 457 (blue), 523 (green), and 590 nm (orange), respectively. The whole shift of the reflectance wavelength is marked in each panel. The inset photographs in panel a are obtained at RH = 20% (violet) and 90% (blue), while those in panels b and c are taken at RH = 90% conditions. (d) UV reflectance profiles at RH = 90% for P(60) and P(76) films, fitted by Macleod package. Refractive index (n) and film thickness (d) are employed as fitting parameters.

were controlled from 29 to 76 mol.% to adjust the hygroscopic properties. The ability to control the SL values would give benefits in optimizing sensor performance. The incorporation of hydrophobic PMB chains is expected to restrain excessive swelling of the films upon exposure to water vapor. In particular, the thermodynamic immiscibility between PSS and PMB chains can create self-assembled morphology, which offers short water diffusion pathways in nanometer scales for hydration and dehydration.

Two hundred forty-nanometer-thick PSS-b-PMB films on Si wafers with native oxide layers were prepared by spin-coating. The morphology of the films beneath the surface in position space was investigated by cross-sectional TEM experiments. In Figure 1b, we show representative cross-sectional TEM images of a P(60) film obtained in dry state, demonstrating well-defined hexagonal cylindrical morphology (HEX) possessing hydrophobic PMB cylinders, dispersed in a hydrophilic PSS matrix. The PSS phases are darken by RuO_4 staining. The equilibrium morphology that obtained in bulk phase is analogous to the thin film morphology with negligible difference in domain size, as shown in the inset figure of Figure 1b. Noted here that the entire PSS-b-PMB samples examined in present study (in the 29−76 mol.% SL range) exhibit qualitatively the same HEX morphologies, with average domain spacings of 21.6 ± 2.9 nm. The HEX morphology comprising a PSS matrix is aimed at the easy access of water molecules in and out of the films. This is in sharp contrast to other block copolymer humidity sensors explored to date where parallel-oriented lamellae were employed.[28,29]

Color-Displaying PSS-b-PMB films upon Exposure to Humidity. P(29), P(35), P(42), P(49), P(60), and P(76) films

with a fixed thickness of ∼240 nm are prepared, as confirmed by a variable-angle multiwavelength ellipsometer. In dry state (RH < 30%), all samples indicate violet reflection color. However, exposing dry films to moist air resulted in visually readable instant color changes, as identified by the naked-eye and UV reflectance experiments.

Typical examples are given in Figure 2 where the data are obtained from P(35), P(60), and P(76) films at room temperature. The UV reflectance of P(35) indicates red shift in the wavelength from 397 to 457 nm upon changing RH from 20 to 90%. Photographs of the P(35) film taken under RH = 20 (violet) and 90% (blue) are shown in the inset figures of Figure 2a, which are in good agreements with the UV results. Interestingly, the shift of reflection wavelength ($\Delta\lambda$) was a sensitive function of SL. When the same experimental protocols are repeated with P(60) and P(76) samples, the reflection colors at RH = 90% were deviated as green and orange, respectively (see inset photographs of Figures 2b and 2c). The $\Delta\lambda$ values of P(60) and P(76) films were 137 and 196 nm, respectively. In Figures 2b and 2c, the UV reflectance profiles of P(60) and P(76) at RH = 90% are plotted, compared to those at RH = 20%.

UV reflectance profiles of PSS-b-PMB films were analyzed using commercially available thin film optic software (Essential Macleod, Thin Film Center Inc.) to underpin the color-displaying behavior. For model fits, we utilized a single layer model for better illustration of HEX morphology with a PSS matrix. The refractive indices of PMB (n_{PMB}) and PS (n_{PS}) are known to be 1.48 and 1.59, respectively,[44] while that of partially sulfonated PSS chains (n_{PSS}) has not clearly discovered in literatures. From ellipsometer experiments on dry films,
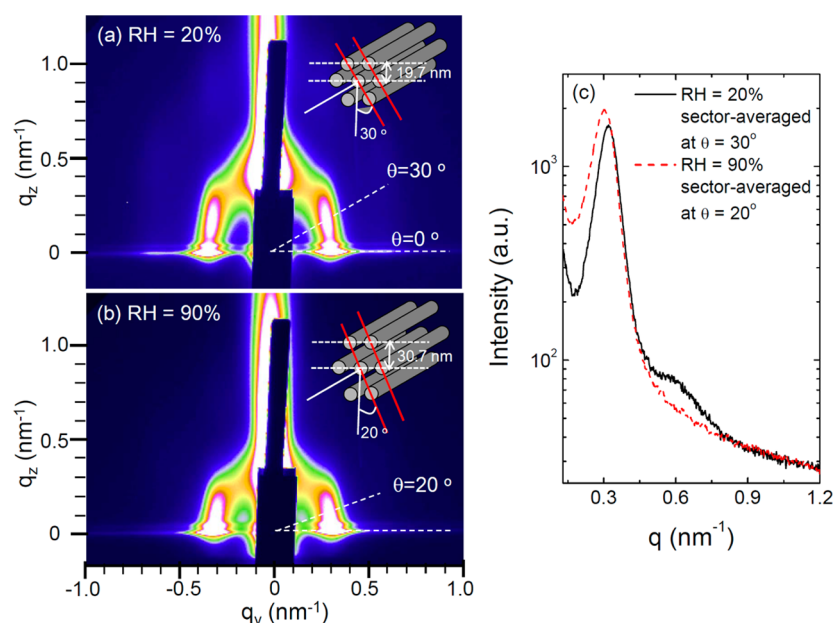
Figure 3. GISAXS intensities of a P(60) film at (a) RH = 20% and (b) RH = 90% conditions (T = 25 °C) as a function of the scattering vectors along the horizontal and vertical direction. Upon exposing the P(60) film to RH=90%, an intriguing distortion of hexagonal symmetry in the 2D scattering pattern is revealed, as illustrated in the inset graphics of b. (c) Sector-averaged GISAXS intensities of the P(60) film at RH = 20 and 90% conditions.

refractive index ($n_{PSS-PMB}$) of PSS-b-PMB was estimated at 1.56 and thus, we can estimate the n_{PSS} using a two-phase structure as follows:

$$n_{PSS-PMB} = \phi_{PMB}n_{PMB} + (1 - \phi_{PMB})n_{PSS} \qquad (2)$$

where ϕ_{PMB} is the volume fraction of PMB domains in the HEX structure, calculated using pure density of each component. The obtained n_{PSS} values in dry state were qualitatively the same as 1.64 for both P(60) and P(76) samples.

Exposing the PSS-b-PMB films to humid air should lead to the decrease in refractive index (n) and the increase in film thickness (d) because of the spontaneous water sorption of PSS phases. The model fits suggest that n = 1.47, d = 360 nm and n = 1.44, d = 410 nm for the hydrated P(60) and P(76) films, respectively. The results imply that the different levels of color changes are attributed to the dissimilar degree of swelling as a function of SL. Representative fitting results of the UV reflectance profiles at RH = 90% for P(60) and P(76) films are shown in Figure 2d.

In Situ GISAXS Experiments on PSS-b-PMB Films. We carried out in situ GISAXS experiments to investigate the changes in morphologies of PSS-b-PMB films as a result of humidification. Figures 3a and 3b show the GISAXS intensities as a function of q_y and q_z, the scattering vectors along the horizontal and vertical directions, respectively (ignoring the shallow angle of grazing incidence), of the P(60) film at RH = 20 and 90%, measured at room temperature. The incident angle of 0.21° above the critical angle of the polymer film (0.16°) was used to determine the morphology through the entire film thickness.

In dry air (RH = 20%), as shown in Figure 3a, we observed parallel oriented HEX domains, as revealed by two strong spots at the azimuthal angles (θ) of 30° and 150°, with high order peaks at 1:2 ratio. This can be attributed to the dominant (100) orientation of HEX structures along the substrate.[46] The domain spacing was 19.7 nm in dry state, which is in good

agreement with the TEM results (Figure 1b). Upon exposing the P(60) film to RH = 90%, as shown in Figure 3b, we see an intriguing distortion of hexagonal symmetry in the 2D scattering pattern. Two spots are appeared at the θ of 20 and 160°, concurrently with the shift of the out-of-plane scattering (at θ = 90°) toward lower q values. This signals that the HEX domains of P(60) film are swelled in anisotropic way, as illustrated in the inset graphics of Figure 3b, due to the confinement effect from the SiO_2/Si-substrate so that lateral swelling of the film is restricted. Figure 3c shows sector-averaged scattering intensities for RH = 20 and 90% at azimuthal positions of 30° and 20°, respectively. High order peak is only evident at RH = 20% conditions since the (100) orientation of HEX strructure is distorted with humidity owing to the anistropic swelling behavior.

By combining the changes in azimuthal angle and out-of-plane domain spacing, the change in film thickness is estimated at 156% upon switching RH from 20% to 90%, which is in excellent agreement with the model fits by Macleod (Figure 2d). We note in passing that when the film is returned back to the dry state, the hexagonal symmetry in 2D scattering pattern is revisited with virtually no difference in domain spacing.

It should be noted here that the presence of moisture leads to a reduction in defect density at the air surface of the sensor, as investigated with small incident angle (0.14°) below the critical angle of the polymer film. For example, randomly organized surface morphology, that is, isotropic ring pattern, was observed for as cast films whereas the ring pattern immediately turned into two-spot pattern with exposure to humid air. Once the surface of the film is composed of long-range ordered cylinders with an aid of humidity, it remains stable since swelling mostly occurs along film thickness direction. The details on the GISAXS patterns illustrating surface phenomena are shown in Figure S2 of Supporting Information.

From these results obtained so far, schematic graphics illustrating the swelling behavior and color-displaying mechanism of HEX-forming PSS-b-PMB sensors are given in Scheme 1. The PSS chains with hygroscopic nature allow the films to

Scheme 1. A schematic illustration of the structure of the PSS-b-PMB humidity sensor and the mechanism of the color changes between low and high RH conditions. The hygroscopic PSS chains spontaneously absorb water from moist air and the swelling changes the film thickness to reflect visible light with different wavelengths
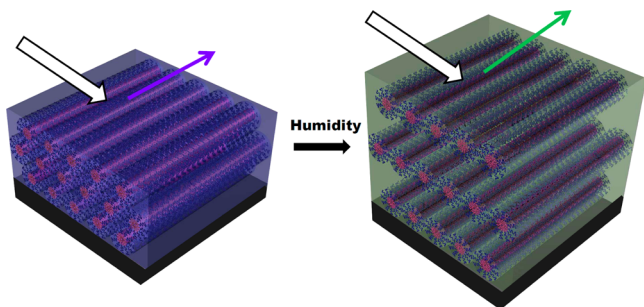
swell in the presence of moisture. The covalently bonded hydrophobic PMB blocks help to retain the film stability during the water absorption by confinement effects in nanometer scales. The swelling changes the film thicknesses and thus causes alteration in the wavelength of visible light reflected by the films. We hypothesized that a unique structural advantage of PSS-b-PMB sensors possessing a PSS matrix would offer easy access of water in and out of the films.

3D RGB Diagrams of PSS-b-PMB Sensors. For the purpose of color-displaying humidity sensors, the sensitivity at a range of RHs is an important parameter, which can be evaluated by the shift of the reflection colors upon switching RHs. To provide moist air with accurate RH values, the PSS-b-

PMB films were placed in humidity/temperature environmental chamber and in situ photographs of the films under levels of humidity were taken via viewing window of the chamber (the photographs are given in Figure S3 of Supporting Information).

At different RHs, the PSS-b-PMB films with different SLs exhibit characteristic reflection colors, which are plotted inside 3-dimensional (3D) cube in Figure 4. The z-axis shows equilibrium water uptake values of 5 μm thick freestanding films where the water uptake is defined as the amounts of water over the weight of dry film. Filled symbols in the 3D cube represent experimental data while the 3D color surface within the cube was obtained using a Renka-Cline gridding algorithm, which is part of the OriginPro 8.5[(R)] software package. Upon creating cross sections of the cube, 2D diagram can illuminate the RH or SL dependent reflection color for our sensors. Representative examples at SL = 76 mol % and RH = 95% are plotted on the right-hand side of the 3D cube. The letters R, O, Y, G, B, and V indicate red, orange, yellow, green, blue, and violet, respectively.

As seen from Figure 4, a large portion of the cube is taken up by blue color for the films with relatively low SL values, while considerable window of color diagram is occupied by green/yellow colors for highly sulfonated samples. What is interesting is that the same color was observed if the samples exhibit similar levels of water uptake. For example, the water uptakes of 55 wt % at RH = 95% (P(42)), 49 wt % at RH = 90% (P(60)), and 50 wt % at RH = 85% (P(76)) yield qualitatively the same green color. It is striking to note that P(76) sample can cover almost entire visible spectrum with RHs ranging from 30 to 95%. This should be a unique advantage over other samples when read humidity values.

Note in passing that the RGB diagrams of our sensor are largely affected by the initial film thickness. For example, upon preparing thicker film, i.e., 340 nm, all sensors indicate green reflection color at low RH < 30%. When humid air is exposed to the green-displaying films, the red-shift in the reflection
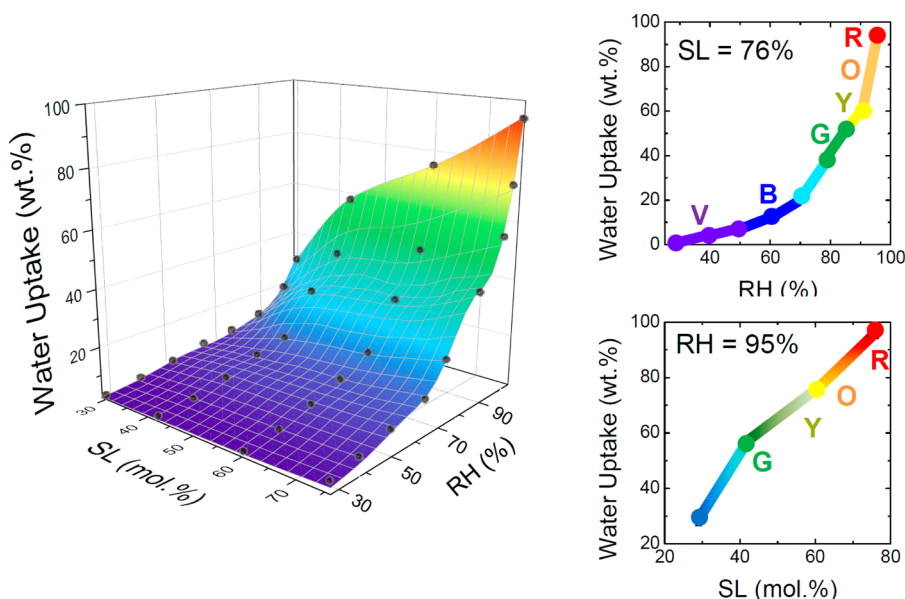
Figure 4. (a) 3-Dimensional phase cube of PSS-b-PMB sensors as a function of relative humidity (RH) and sulfonation level (SL). The z-axis indicates water uptakes to illustrate the degree of swelling of each sensor. Filled symbols represent experimental data while the 3D color surface within the cube was obtained using a Renka-Cline gridding algorithm. Cross-sectional 2D color diagrams at SL = 76 mol % and RH = 95% are given in the right-hand side of the cube.
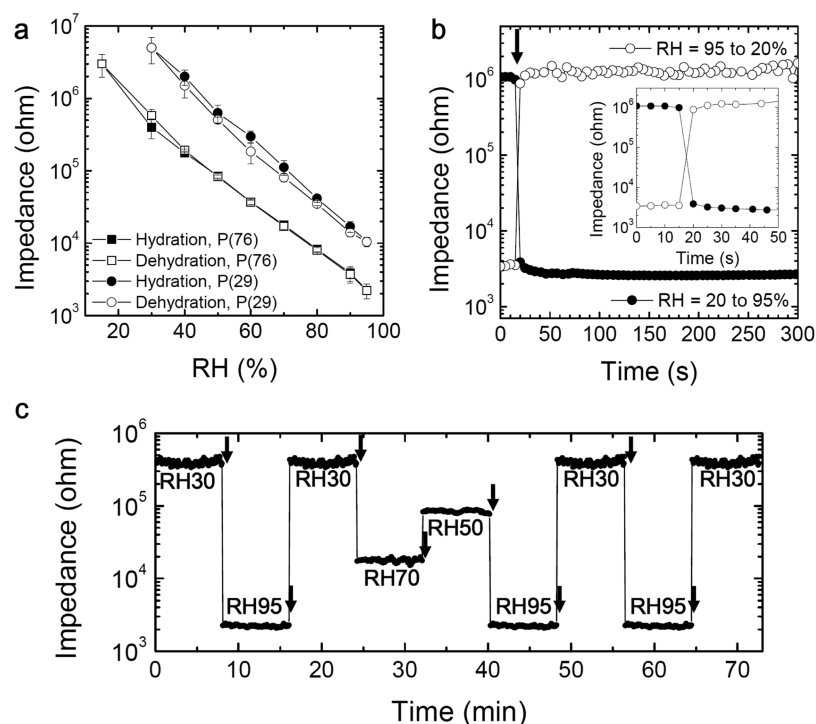
Figure 5. (a) Calibration curves and hysteresis loop of impedance for P(29) and P(76) films, obtained with repeated hydration/dehydration cycles at 25 °C. (b) The impedance variation with time for a P(76) film upon switching RHs between 20 and 95% at 25 °C. Quantitative response time to impedance variation was obtained as 5 s for both hydration and dehydration, as shown in the inset figure. (c) Impedance changes of a P(76) film, monitored with repeated stepwise changes in RHs. For all measurements, an AC voltage of 20 mV at a fixed frequency of 1 kHz was supplied. The injection of air with different RHs was indicated in the figure with inverted arrows.

peaks was again detected; the sensor from a 340 nm thick P(76) film showed reflection colors of green (RH < 30%), yellow (RH = 40%), orange (RH = 45%), red (RH = 50%), and coloress (RH=55%). This indicates that the increase in film thickness enables us to measure relatively low RH values precisely whereas the limited readibility of high RH values becomes problematic.

What is most interesting is that for all samples, the time to complete the changes in color was approximately 2 s, regardless of the RH gradient where the colors remained stable with extended exposure time up to 2 months. The dehydration behavior bears resemblance to that of hydration. In Figure S4 of Supporting Information, we show a movie demonstrating the fast and reproducible color changes among RH = 30, 80, and 90% for a P(60) film. This implies that the water sorption and desorption of the PSS-b-PMB films are radically fast, which could be intimately related to the well-connected hydrophilic PSS matrices of HEX structures. To verify this hypothesis, a lamellar-forming PSS-b-PMB film (PSS content was low as 45 vol.%) was pepared to test the colorimetric response to humidity (data not shown here). To our surprise, although the sample exhibits capability to detect humidity with substantial changes in color, considerably slow response time over 30 s was detect. This clearly signals that easy access of water molecules into the hydrophilic PSS domains plays a central role in determining response time of our sensor.

It is also worthwhile to note that when PSS homopolymers were employed for humidity sensors, even with SL = 30 mol. %, the films exhibit hole and island structures with prolonged exposure to moisture. The exclusive stability and reversibility in the color changes of PSS-b-PMB sensors should be originated

from the structural integrity of PSS-b-PMB films, as demonstrated by GISAXS experiments (Figure 3).

Resistive PSS-b-PMB Films under Levels of Humidity. We explored a dual-functionality of our PSS-b-PMB sensors to describe the ramifications of our work over the vast body of polymeric humidity sensors, reported to date. The sensors from PSS-b-PMB films offer large changes in electrochemical properties upon exposure to moisture since the existence of water molecules in pools of $-SO_3H$ groups leads to proton transports along neighboring protic moieties, yielding a decrease in impedance of the films.

We first made calibration curves and hysteresis loop of impedance, as measured by repeated hydration/dehydration cycles at 25 °C. An ac voltage of 20 mV at a single frequency of 1 kHz was applied to measure impedance of our sensors with humidity. The frequency of 1 kHz was located in impedance plateau region of PSS-b-PMB films. The representative data are shown in Figure 5a where the data are obtained from P(29) and P(76) films. As can be seen from Figure 5a, relatively wide ranges of RH and impedance variation were observed with P(76) sensor, compared with P(29), because of the enhanced ionic strength of the highly sulfonated sample. It is evident that the quantitative determination of RH values becomes feasible, if our sensors are in the resistive mode (colorimetric mode is a relatively qualitative method to detect RHs). From the small hysteresis loop of impedance for both P(29) and P(76) samples, we can infer that the dehydration behavior bears resemblance to that of hydration on analogy to the colorimetric response.

The changes in impedance of PSS-b-PMB sensors were then monitored with stepwise changes in RHs at 25 °C. Figure 5b shows the impedance of a P(76) film with time upon switching

Table 1. Color Change, Impedance Variation, and Response Time of Humidity Sensors Reported in the Literature and Observed in Present Study

materials used	color change (Δλ, nm)	impedance variation (Ω)	response time (s)	RH range (%)	ref
CdS nanoparticles		$8 \times 10^{10} - 1 \times 10^8$	60	17−85	47
Au/Pd nanofibers		a	>60	11−94	48
ZnO nanocrystals		a	50	5−85	15
CuO/ZnO nanocorals		$1 \times 10^7 - 4 \times 10^3$	6−8	33−90	49
porous TiO$_2$		$1 \times 10^5 - 1 \times 10^1$	10	11−95	50
Al$_2$O$_3$ nanotubes		$2 \times 10^4 - 3 \times 10^1$	>10	11−95	8
Na-ZnO nanofiber		$4 \times 10^7 - 2 \times 10^3$	5	11−95	51
polyaniline nanofibers		$8 \times 10^6 - 3 \times 10^3$	6−8	11−98	52
cross-linked polyelectrolyte derivatives		$2 \times 10^6 - 4 \times 10^2$	125	20−95	53
sulfonated polystyrene		$5 \times 10^5 - 6 \times 10^3$	>300	25−95	54
TiO$_2$ incorporated sulfonated polystyrene		$1 \times 10^7 - 4 \times 10^3$	50	11−95	55
sulfonated polyimides		$1 \times 10^5 - 5 \times 10^1$	70	30−90	56
polyaniline/polystyrene		$3 \times 10^3 - 1 \times 10^3$	a	0−90	22
TiO$_2$/SiO$_2$ Bragg stacks	11		a	40−80	3
latex spheres photonic crystals	240		a	20−100	57
Au nanorod embedded polymer nanofibers	11.5		0.11	30−71	58
cholesteric liquid crystals	40		600	3−83	59
fluorophore in hydrogels	40		>10	0−100	20
magnetic polymer gel photonic crystals	153		>100	11−97	60
PEG-diacrylate photonic crystals	137		a	25−98	61
nanoporous polymeric photonic crystals	b		1.5	40−95	62
sulfonated block copolymers	196		2	30−95	present study
		$3 \times 10^6 - 2 \times 10^3$	5	15−95	present study

[a]The information is unknown in the literature. [b]Relative transmittance is given.

RH from 20 to 95%. The injection of humid/dry air is marked with the inverted arrow. As can be seen from the figure, 3 orders of magnitude decrease in impedance was recorded with time where the time to complete the impedance change was found out to be only 5 s. Upon restoring RH to 20%, the impedance value of the P(76) film was returned back to the initial value within 5 s.

In Figure 5c, comprehensive sensitivity data are provided with repeated discontinuous RH changes. The injection of air with different RHs is marked with inverted arrows. It is evident that regardless RH gradients, changes in RHs among 30, 50, 70, and 95% cause steep alterations in the impedance with exceptionally fast response time of 5 s. The overall trend observed with other samples possessing different SLs is qualitatively similar to that with P(76) film although the degree of impedance changes is depending on the SLs. To the best of our knowledge, our systems revealed the superior response time to other polymeric humidity sensors, reported in literatures. Such fast response time should be the most important parameter in evaluating the sensor performance.

We made comparison of humidity sensor performance reported in literatures and observed in present study, as summarized in Table 1. We examined both polymeric materials and a wide variety of inorganic materials. As shown in Table 1, while polymeric humidity sensors have unique advantages of flexibility, large-scale production, and low cost, most of them revealed slower response times to impedance changes than those of inorganic materials. In contrast, it is evident that our sensors demonstrated fast response time to the impedance changes. Regarding the colorimetric behavior, our sensors exhibited relatively large shifts in reflection wavelength, which is comparable to the best performance reported in the literature. The fast response time of 2 s to color changes should be noteworthy. Particularly, as can be seen from Table 1, to the best of our knowledge, no paper has reported dual-mode humidity sensor in which both modes reveal the top level of performance.

We hope conclude our paper by commenting on the temperature effects on the dual-mode performance of our sensors. With temperature variation from 25 to 50 °C, no major change in reflection color was detected with the naked eye. This is due to the fact that there are negligible changes in water uptakes of PSS-b-PMB films in that temperature regime.[43] However, the increase in temperature results in the decrease in impedance, following the well-known Arrhenius relationship, due to the enhanced proton transport rate at high temperature. Although the absolute impedance values are affected by temperature, the main conclusions on the performance of our sensors are not altered, in aspects of high sensitivity with RH gradients, small hysteresis loop of impedance, and fast response time. The structural stability of our sensors at high temperature was also demonstrated by in situ small angle neutron scattering experiments (see Figure S5 of Supporting Information).

The development of dual-mode thin film humidity sensors with fast response and good sensitivity via rational structural designs would open promising avenues toward microsensor applications. It is also envisaged that the present systems would be applicable to other types of chemical vapors (ammonia and warfare agents) with rapid detection.

■ CONCLUSION

We developed a simple but powerful system toward real-time humidity monitoring with high susceptibility. The nano-structured PSS-b-PMB films exhibited visually readable color changes in a range of RH from 20 to 90% where the whole shift of reflectance wavelength was 196 nm. The PSS-b-PMB sensors have also shown promise for detecting humidity with high sensitivity by monitoring electrochemical properties on account

of strong polymer electrolytes characteristics. The time to complete the changes in color and impedance was only a few seconds, attributed to the unique structural advantage of HEX-forming PSS-b-PMB sensors that offers easy access and short diffusion pathways of water molecules in nanometer scales. This is in sharp contrast to other sulfonated polymers reported in the literatures, such as Nafion, where the structural designs were not practicable.

■ ASSOCIATED CONTENT

Ⓢ Supporting Information

Schematic drawing of interdigitated gold electrode, GISAXS intensities representing the change in surface morphology with humidity, in situ photographs of the sensors under levels of humidity, a video demonstrating the fast and reproducible color changes, and in situ SANS profiles confirming structural stability of our sensor at high temperatures. This information is available free of charge via the Internet at http://pubs.acs.org/.

■ AUTHOR INFORMATION

Corresponding Author
*E-mail: moonpark@postech.edu.

Notes

The authors declare no competing financial interest.

■ ACKNOWLEDGMENTS

■ REFERENCES

(1) Stuart, M. A. C.; Huck, W. T. S.; Genzer, J.; Müller, M.; Ober, C.; Stamm, M.; Sukhorukov, G. B.; Szleifer, I.; Tsukruk, V. V.; Urban, M.; Winnik, F.; Zauscher, S.; Luzinov, I.; Minko, S. *Nat. Mater.* **2010**, *9*, 101−113.

(2) Ramesh, G. V.; Radhakrishnan, T. P. *ACS Appl. Mater. Interfaces* **2011**, *3*, 988−994.

(3) Pavlichenko, I.; Exner, A. T.; Guehl, M.; Lugli, P.; Scarpa, G.; Lotsch, B. V. *J. Phys. Chem. C* **2012**, *116*, 298−305.

(4) Arai, H.; Seiyama, T. *Sensors: A Comprehensive Survey, Chemical and Biochemical Sensors Part II*; Wiley: New York, 1991.

(5) Luechinger, N. A.; Locher, S.; Athanassiou, E. K.; Grass, R. N.; Stark, W. J. *Langmuir* **2007**, *23*, 3473−3477.

(6) Zampetti, E.; Pantalei, S.; Pecora, A.; Valletta, A.; Maiolo, L.; Mintoti, A.; Macagnano, A.; Fortunato, G.; Bearzotti, A. *Sens. Actuators, B* **2009**, *143*, 302−307.

(7) Hao, Y.; Meng, G.; Ye, C.; Zhang, L. *Appl. Phys. Lett.* **2005**, *87*, 033106−3.

(8) Cheng, B.; Tian, B.; Xie, C.; Xiao, Y.; Lei, S. *J. Mater. Chem.* **2011**, *21*, 1907−1912.

(9) Kuang, Q.; Lao, C.; Wang, Z. L.; Xie, Z.; Zheng, L. *J. Am. Chem. Soc.* **2007**, *129*, 6070−6071.

(10) Beliatis, M. J.; Martin, N. A.; Leming, E. J.; Silva, S. R. P.; Henley, S. J. *Langmuir* **2011**, *27*, 1241−1244.

(11) Zhang, J.; Shen, G.; Wang, W.; Zhou, X.; Guo, S. *J. Mater. Chem.* **2010**, *20*, 10824−10828.

(12) Kashi, M. A.; Ramazani, A.; Abbasian, H.; Khayyatian, A. *Sens. Actuators, A* **2012**, *174*, 69−74.

(13) Wang, Z.; Li, Z.; Sun, J.; Zhang, H.; Wang, W.; Zheng, W.; Wang, C. *J. Phys. Chem. C* **2010**, *114*, 6100−6105.

(14) Li, Z.; Zhang, H.; Zheng, W.; Wang, W.; Huang, H.; Wang, C.; MacDiarmid, A. G.; Wei, Y. *J. Am. Chem. Soc.* **2008**, *130*, 5036−5037.

(15) Hu, X.; Gong, J.; Zhang, L.; Yu, J. C. *Adv. Mater.* **2008**, *20*, 4845−4850.

(16) Ashley, G. M.; Kirby, P. B.; Butler, T. P.; Whatmore, R.; Luo, J. K. *J. Electrochem. Soc.* **2010**, *157*, J419−J424.

(17) Buvailo, A. I.; Xing, Y.; Hines, J.; Dollahon, N.; Borquet, E. *ACS Appl. Mater. Interfaces* **2011**, *3*, 528−533.

(18) Barry, R. A.; Wiltzius, P. *Langmuir* **2006**, *22*, 1369−1374.

(19) Evans, R. C.; Douglas, P. *ACS Appl. Mater. Interfaces* **2009**, *1*, 1023−1030.

(20) Tellis, J. C.; Strulson, C. A.; Myers, M. M.; Kneas, K. A. *Anal. Chem.* **2011**, *83*, 928−932.

(21) Galindo, F.; Lima, J. C.; Luis, S. V.; Melo, M. J.; Parola, A. J.; Pina, F. *J. Mater. Chem.* **2005**, *15*, 2840−2847.

(22) Matsuguchi, M.; Yamanaka, T.; Yoshida, M.; Kojima, S.; Okumura, S. *J. Electrochem. Soc.* **2009**, *156*, J299−J302.

(23) Wang, X.; Ding, B.; Yu, J.; Wang, M. *J. Mater. Chem.* **2011**, *21*, 16231−16238.

(24) Sun, A.; Wang, Y.; Li, Y. *Sens. Actuators, B* **2010**, *145*, 680−684.

(25) Choi, I.; Ahn, H.; Park, M. J. *Macromolecules* **2011**, *44*, 7327−7334.

(26) Zhang, L.; Chaloux, B. L.; Saito, T.; Hickner, M. A.; Lutkenhaus, J. L. *Macromolecules* **2011**, *44*, 9723−9730.

(27) Weber, J.; Kreuer, K.-D.; Maier, J.; Thomas, A. *Adv. Mater.* **2008**, *20*, 2595−2598.

(28) Kang, Y.; Walish, J. J.; Gorishnyy, T.; Thomas, E. L. *Nat. Mater.* **2007**, *6*, 957−960.

(29) Ayyub, O. B.; Sekowski, J. W.; Yang, T. I.; Zhang, X.; Briber, R. M.; Kofinas, P. *Biosens. Bioelectro.* **2011**, *28*, 349−354.

(30) Mishra, H.; Misra, V.; Mehata, M. S.; Pant, T. C.; Tripathi, H. B. *J. Phys. Chem. A* **2004**, *108*, 2346−2352.

(31) Su, P.-G.; Huang, L.-N. *Sens. Actuators, B* **2007**, *123*, 501−507.

(32) Zhou, Y.; Grunwaldt, J.-D.; Krumeich, F.; Zheng, K.; Chen, G.; Stötzel, J.; Frahm, R.; Patzke, G. R. *Small* **2010**, *6*, 1173−1179.

(33) Venditti, I.; Fratoddi, I.; Bearzotti, A. *Nanotechnology* **2010**, *21*, 355502.

(34) Hawkeye, M. M.; Brett, M. J. *Adv. Funct. Mater.* **2011**, *21*, 3652−3658.

(35) Ge, J.; Yin, Y. *Angew. Chem., Int. Ed.* **2007**, *46*, 4342−4345.

(36) Arsenault, A. C.; Puzzo, D. P.; Manners, I.; Ozin, G. A. *Nat. Photonics* **2007**, *1*, 468−472.

(37) Zhao, Y.-J.; Zhao, X.-W.; Hu, J.; Li, J.; Xu, W.-Y.; Gu, Z.-Z. *Angew. Chem., Int. Ed.* **2009**, *48*, 7350−7352.

(38) Aguirre, C. I.; Reguera, E.; Stein, A. *Adv. Funct. Mater.* **2010**, *20*, 2565−2578.

(39) Garcia, P. D.; Sapienza, R.; Lopez, C. *Adv. Mater.* **2010**, *22*, 12−19.

(40) Ruminski, A. M.; Moore, M. M.; Sailor, M. J. *Adv. Funct. Mater.* **2008**, *18*, 3418−3426.

(41) Moon, J. H.; Yang, S. *Chem. Rev.* **2010**, *110*, 547−574.

(42) Wang, Z.; Zhang, J.; Xie, J.; Li, C.; Li, Y.; Liang, S.; Tian, Z.; Wang, T.; Zhang, H.; Li, H.; Xu, W.; Yang, B. *Adv. Funct. Mater.* **2010**, *20*, 3784−3790.

(43) Park, M. J.; Downing, K. H.; Jackson, A.; Gomez, E. D.; Minor, A. M.; Cookson, D.; Weber, A. Z.; Balsara, N. P. *Nano Lett.* **2007**, *7*, 3547−3552.

(44) Park, M. J.; Balsara, N. P. *Macromolecules* **2008**, *41*, 3678−3687.

(45) Kim, S. Y.; Kim, S.; Park, M. J. *Nat. Commun.* **2010**, *1*, 88.

(46) Park, M. J.; Kim, S.; Minor, A.; Balsara, N. P. *Adv. Mater.* **2009**, *21*, 203−208.

(47) Dermir, R.; Okur, S.; Seker, M. *Ind. Eng. Chem. Res.* **2012**, *51*, 3309−3313.

(48) Jia, W.; Wang, Y.; Basu, J.; Strout, T.; Carter, B.; Gokirmak, A.; Lei, Y. *J. Phys. Chem. C* **2009**, *113*, 19525−19530.

(49) Zainelabdin, A.; Amin, G.; Zaman, S.; Nur, O.; Lu, J.; Hultman, L.; Willander, M. *J. Mater. Chem.* **2012**, *22*, 11583−12590.

(50) Wang, Z.; Shi, L.; Wu, F.; Yuan, S.; Zhao, Y.; Zhang, M. *Nanotechnology* **2011**, *22*, 275502.

(51) Zhang, H.; Li, Z.; Wang, W.; Wangw, C. *J. Am. Ceram. Soc.* **2010**, *93*, 142−146.

(52) Lin, Q.; Li, Y.; Yang, M. *Sens. Actuators, B* **2012**, *171−172*, 309−314.

(53) Lee, C.-W.; Joo, S.-W.; Gonga, M.-S. *Sens. Actuators, B* **2005**, *105*, 150−158.

(54) Rubinger, C. P. L.; Martins, C. R.; Paoli, M.-A. D.; Rubinger, R. M. *Sens. Actuators, B* **2007**, *123*, 42−49.

(55) Sun, A.; Haung, L.; Li, Y. *Sens. Actuators, B* **2009**, *139*, 543−547.

(56) Ueda, M.; Nakamura, K.; Tanaka, K.; Kita, H.; Okamoto, K. *Sens. Actuators, B* **2007**, *127*, 463.

(57) Tian, E.; Wang, J.; Zheng, Y.; Song, Y.; Jiang, L.; Zhu, D *J. Mater. Chem.* **2008**, *18*, 1116−1122.

(58) Wang, P.; Zhang, L.; Xia, Y.; Tong, L.; Xu, X.; Ying, Y. *Nano Lett.* **2012**, *12*, 3145−3150.

(59) Herzer, N.; Guneysu, H.; Davies, D. J. D.; Yildirim, D.; Vaccaro, A. R.; Broer, D. J.; Bastiaansen, C. W. M.; Schenning, A. P. H. J. *J. Am. Chem. Soc.* **2012**, *134*, 7608−7611.

(60) Hu, H.; Chen, Q.-W.; Chengb, K.; Tang, J. *J. Mater. Chem.* **2012**, *22*, 1021−1027.

(61) Kim, J. H.; Moon, J. H.; Lee, S.-Y.; Park. *Appl. Phys. Lett.* **2010**, *97*, 103701−3.

(62) Shi, J.; Hsiao, V. K. S.; Walker, T. R.; Huang, T. J. *Sens. Actuators B* **2008**, *129*, 391−396.

5187

dx.doi.org/10.1021/am3011115 | *ACS Appl. Mater. Interfaces* 2012, 4, 5179−5187